Title
Enhanced surface photochemistry in chloride-nitrate ion mixtures.

Journal
Physical chemistry chemical physics : PCCP, 10(37)

ISSN
1463-9076

Authors
Wingen, Lisa M
Moskun, Amy C
Johnson, Stanley N
et al.

Publication Date
2008-10-01

Peer reviewed

PCCP

Physical Chemistry Chemical Physics

www.rsc.org/pccp

Volume 10 | Number 37 | 1 October 2008 | Pages 5641–5788

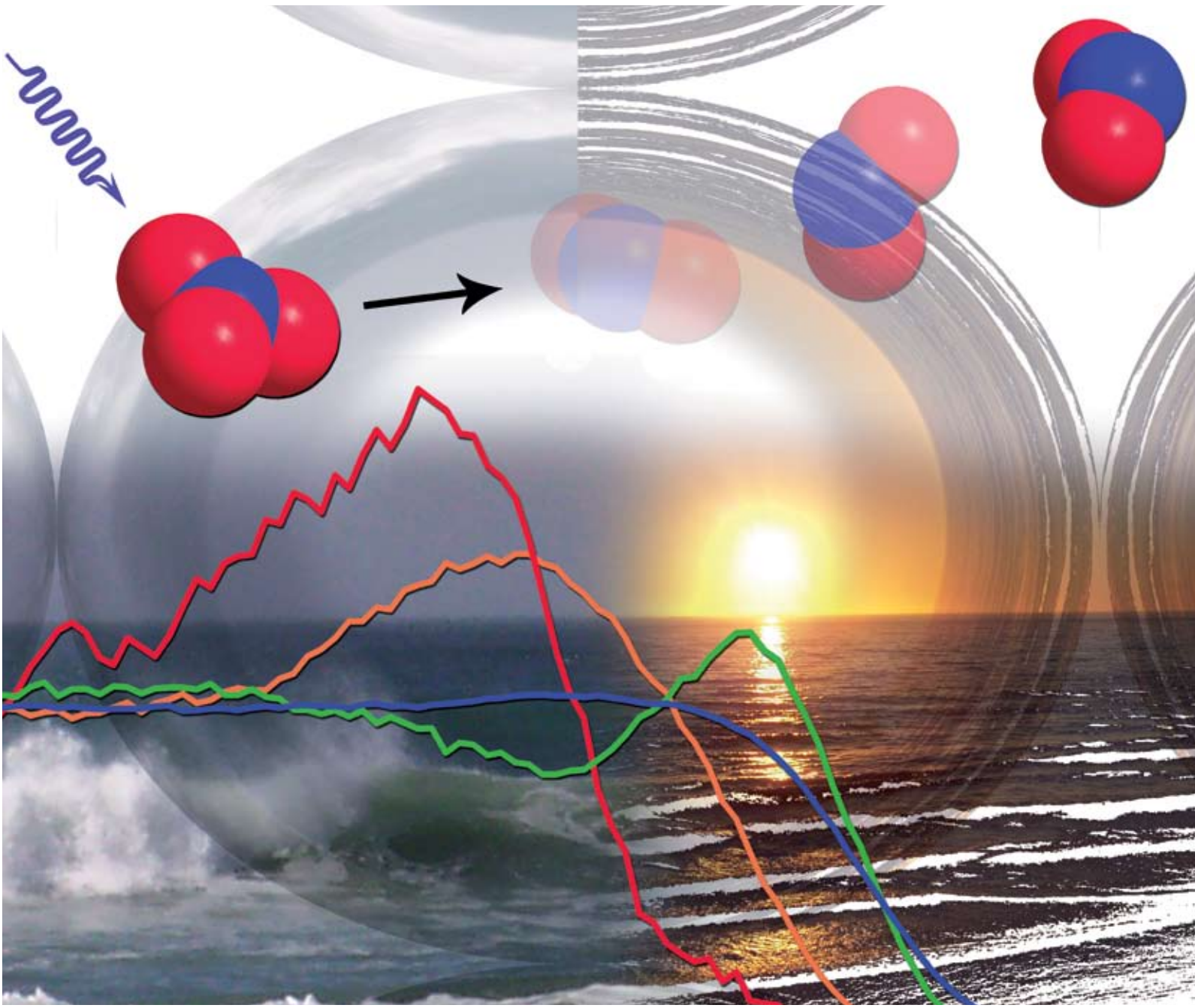

ISSN 1463-9076

COVER ARTICLE
Wingen *et al.*
Enhanced surface photochemistry in chloride–nitrate ion mixtures

PERSPECTIVE
Blumberger
Free energies for biological electron transfer from QM/MM calculation

1463-9076(2008)10:37;1-V

Enhanced surface photochemistry in chloride–nitrate ion mixtures†

Lisa M. Wingen,[a] Amy C. Moskun,‡[a] Stanley N. Johnson,[a] Jennie L. Thomas,[a] Martina Roeselová,[b] Douglas J. Tobias,[a] Michael T. Kleinman[c] and Barbara J. Finlayson-Pitts*[a]

Received 18th April 2008, Accepted 5th June 2008
First published as an Advance Article on the web 28th July 2008
DOI: 10.1039/b806613b

Heterogeneous reactions of sea salt aerosol with various oxides of nitrogen lead to replacement of chloride ion by nitrate ion. Studies of the photochemistry of a model system were carried out using deliquesced mixtures of NaCl and $NaNO_3$ on a Teflon® substrate. Varying molar ratios of NaCl to $NaNO_3$ (1 : 9 Cl^- : NO_3^-, 1 : 1 Cl^- : NO_3^-, 3 : 1 Cl^- : NO_3^-, 9 : 1 Cl^- : NO_3^-) and $NaNO_3$ at the same total concentration were irradiated in air at 299 ± 3 K and at a relative humidity of 75 ± 8% using broadband UVB light (270–380 nm). Gaseous NO_2 production was measured as a function of time using a chemiluminescence NO_y detector. Surprisingly, an enhanced yield of NO_2 was observed as the chloride to nitrate ratio increased. Molecular dynamics (MD) simulations show that as the Cl^- : NO_3^- ratio increases, the nitrate ions are drawn closer to the interface due to the existence of a double layer of interfacial Cl^- and subsurface Na^+. This leads to a decreased solvent cage effect when the nitrate ion photodissociates to $NO_2 + O^{\bullet -}$, increasing the effective quantum yield and hence the production of gaseous NO_2. The implications of enhanced NO_2 and likely OH production as sea salt aerosols become processed in the atmosphere are discussed.

1. Introduction

Sea salt aerosols are known to undergo heterogeneous reactions with gaseous nitrogen oxides (N_2O_5, NO_2, HNO_3, $ClONO_2$), resulting in chloride depletion as they travel through polluted regions.[1–15] The particle composition has been observed to range from no Cl^- depletion (fresh sea salt) to complete Cl^- depletion (heavily processed sea salt), and a strong anti-correlation of Cl^- with NO_3^- has been reported.[4,7,8] As a result, the ratio of Cl^- to NO_3^- in sea salt-derived aerosol decreases as air masses move downwind in coastal urban regions.

While nitrate ions are often treated as a stable end product of this chemistry, NO_3^- absorbs light in the actinic region above 290 nm and photodissociates *via* two reaction channels:[16]

$$NO_3^- + h\nu \rightarrow NO_2 + O^{\bullet -} \xrightarrow{H_2O} NO_2 + OH + OH^- \quad (1a)$$

$$\rightarrow NO_2^- + O(^3P) \quad (1b)$$

The aqueous phase quantum yields are ~0.9% for OH (1a) and ~0.1% for $O(^3P)$ (1b) at 305 nm and 298 K.[16–21] This photochemistry is believed to be important in the Arctic and Antarctic snowpacks, generating NO_x as well as OH and $O(^3P)$ which can carry out subsequent oxidations.[22–25]

Less is known about the photochemistry of nitrate in complex aerosol mixtures, such as in processed sea salt aerosols. Sea salt particles, whether processed or unprocessed, are likely to exist as concentrated aqueous droplets at ambient relative humidities.[26,27] Recently Hudson *et al.*[28] showed that as $Ca(NO_3)_2$ solutions become highly concentrated, the lowest energy electronic absorption peak shifts to higher energy. In addition to the blue shift, the extinction coefficient was shown to decrease by ~30% in moving from dilute (~0.1 M) to highly concentrated (~7 M) solutions. Smaller blue shifts (2–4 nm) were reported to occur for highly concentrated $Mg(NO_3)_2$ and $NaNO_3$ solutions.[28] These results suggest that the overlap of the nitrate absorption spectrum with solar radiation may decrease at the concentrations likely to be found in aerosols. However, it is not known how the UV absorption spectrum of NO_3^- is affected by the presence of Cl^-, such as in processed sea salt particles.

Molecular dynamics (MD) simulations provide a fundamental understanding of the interactions of ions with their solvent at the atomic level. MD simulations have shown that a significant population of Cl^- resides at the interface of aqueous NaCl systems.[29–32] These simulations have been applied to understanding surface-active mechanisms for halogen formation from sea salt aerosols[32–36] and other physicochemical processes at air–water interfaces with very good experimental agreement.[31,37–41] Recent simulations show that nitrate ions in larger particles appear to reside below the interface in pure aqueous

[a] *Department of Chemistry, University of California, Irvine, CA 92697-2025, USA. E-mail: bjfinlay@uci.edu; Fax: 949-824-2420; Tel: 949-824-7670*
[b] *Center for Biomolecules and Complex Molecular Systems, Institute of Organic Chemistry and Biochemistry, Academy of Sciences of the Czech Republic, Flemingovo nam. 2, Prague 6, 16610, Czech Republic*
[c] *Department of Medicine/Occupational & Environmental Medicine, University of California, Irvine, CA 92697-1825, USA*
† Electronic supplementary information (ESI) available: Additional kinetics model details. See DOI: 10.1039/b806613b
‡ Present address: Department of Chemistry, Whittier College, Whittier, CA 90608, USA.

$NaNO_3$ and $Mg(NO_3)_2$ solutions with no particular preference to be solvated at surface.[42–44] However, the small number of nitrate ions that do reside near the interface in pure $NaNO_3$ solutions are under-coordinated by water molecules.[43] In addition, in clusters of up to 300 water molecules, nitrate ions are found to reside primarily near the surface of the cluster and to be under-coordinated by water.[45] Such reduced solvent cages may result in enhanced quantum yields at the interface.[46–50] For example, the photolysis of $Mo(CO)_6$ was observed to be at least three orders of magnitude faster when dispersed in droplets compared to that for the bulk solution.[51]

In the case of nitrate–chloride ion mixtures, the OH radical generated in reaction (1a) can potentially oxidize chloride ions to Cl_2. However, the kinetics and mechanism of this oxidation depend on whether it occurs at the interface or in the bulk. The interface reaction does not involve acid and is fast,[32,52] while the bulk reaction occurs at a significant rate only under acidic conditions.[53] Petriconi *et al.*,[54] in experiments carried out on bulk solutions, showed that the formation of nitrite from sunlight-irradiated $NaNO_3$ solutions increased in the presence of Cl^-. The authors suggested that the presence of Cl^- enhances NO_3^- photolysis through formation of the NOCl intermediate and proposed that the photolysis of nitrate could oxidize halides in marine aerosols. More recently, UV irradiation of particles collected in marine environments has shown that NO_3^- photolysis is a major source of OH radicals in such particles.[55,56]

The present studies describe the generation of gaseous NO_2 upon irradiation of deliquesced $NaNO_3$ compared to mixtures of NaCl and $NaNO_3$ deposited on a Teflon® substrate. The UV/visible absorption spectra of these mixtures were measured to investigate changes in the NO_3^- absorption in concentrated mixtures of NaCl and $NaNO_3$. MD simulations were carried out on mixtures of NaCl and $NaNO_3$ to understand solvation and interfacial concentrations in the two-component system. The combination of experiments and simulations shows that nitrate ions are, on average, closer to the interface when chloride ions are present, leading to more efficient production of gaseous NO_2 due to enhanced photochemistry.

2. Materials and methods

Photolysis experiments

Experiments were performed by coating Teflon® reaction chambers with a thin film of $NaNO_3$/NaCl, and following the generation of gaseous NO_y with time during irradiation. The walls of the reaction chamber were coated with aerosol by nebulizing a solution into the chamber for 6.5 min and then pumping out the chamber. Aerosol particles were generated using a 6-jet Collison nebulizer (BGI Inc., Model CN25) containing aqueous solutions of 4 M total salt concentration (varying the amounts of NaCl and $NaNO_3$; see below) with nitrogen gas at a pressure of 20 psi. This process was repeated three times, leaving a layer of aerosol particles coating the walls of the chamber. The reaction chamber was then filled with air to 55 L through a water bubbler, resulting in initial relative humidities of $\geq 75\%$ at the beginning of all experiments. This approach of using a wall coating rather than suspended particles was used because the unavoidable static charge that develops on Teflon® leads to rapid uptake of particles on the walls of the chamber during the course of a typical experiment, complicating data interpretation. In addition, because the particles remain on the walls, this method avoids removing particles when sampling for gaseous product formation. A new chamber of equal dimensions ($\sim 70 \times 80$ cm) and volume was created for each experiment from FEP Teflon® which was rinsed with Milli-Q water and dried before sealing. Each chamber had Teflon® sampling ports for NO_x measurements and a relative humidity/temperature probe (Vaisala, HMP 338).

Irradiation experiments included pure $NaNO_3$ and mixtures of NaCl and $NaNO_3$ in molar ratios of 1 : 9, 1 : 1, 3 : 1 and 9 : 1, all prepared from salt solutions with a total molarity of 4.0 M (*e.g.* 9 : 1 NaCl : $NaNO_3$ corresponds to 3.6 M NaCl, 0.4 M $NaNO_3$; 1 : 1 NaCl : $NaNO_3$ corresponds to 2.0 M NaCl, 2.0 M $NaNO_3$, *etc.*). In separate experiments, an aerodynamic particle sizer with a 100× diluter (TSI, APS model 3321, diluter model 3302A) was used to determine the particle size and number density of the different salt mixtures used to coat the chambers. Each 6.5 min aerosol nebulizing treatment produced (1–2) $\times 10^6$ particles cm^{-3} with mean aerodynamic diameter $\sim 0.9 \pm 0.1$ μm ($\sigma = 1.4$) for both pure and mixed salts. These particle measurements were carried out to ensure that equal aerosol particle sizes and concentrations were present as the ratio of chloride to nitrate changed. While these sizes are typical of both processed and unprocessed sea salt particles in air,[8] some coalescence of particles on the Teflon® surface occurred to give larger particles. The aerosol layer contained 2–4 mmol of salt, calculated from measurements of mass and published water activity data.[57] The thickness of the layer formed by deposition of the particles was estimated to be 30–50 μm based on the mass of added salt and assuming the film was equally distributed over the surface area of the chamber. Calculations show that less than 3% of the nitrate was photolyzed during an experiment.

Each coated chamber was irradiated from above using a set of 8 UVB lamps ($\lambda \sim 270$–380 nm, UVP Inc., 15 W) with excellent spectral overlap with the lowest energy electronic absorption of aqueous nitrate as shown in Fig. 1.

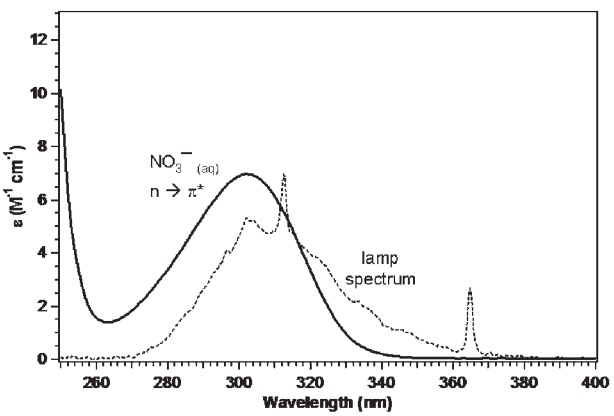

Fig. 1 Absorption spectrum of dilute aqueous $NaNO_3$ (0.4 M, solid line) and photolysis lamp spectrum (dashed line, relative *y*-axis).

Measurements of NO_2 and NO were taken before irradiation, as well as at 15–45 min intervals for 3–4 h using a nitrogen oxides analyzer with chemiluminescence detection (Monitor Labs, Model 8840). The NO_y analyzer was calibrated in the range of NO and NO_2 levels detected in the experiments using known mixtures of NO and NO_2 in nitrogen or air.

A temperature rise of 3–4 °C occurred during the experiments, resulting in the relative humidity decreasing to ~65% RH in some cases. Although mixtures of NaCl and $NaNO_3$ are known to deliquesce at 67%, they do not effloresce until 35% RH or lower.[26,58,59] Similarly, while pure $NaNO_3$ deliquesces at 74.5% RH, it effloresces at <30% RH.[57] Thus, all particles remained deliquesced throughout the experiments, as confirmed by visual inspection.

Computational methods

Simulations of the liquid–vapor interface of aqueous $NaNO_3$ and mixtures of $NaNO_3$ and NaCl were completed using classical molecular dynamics simulations of ions in a box of 864 water molecules. In order to simulate the liquid–vapor interface, a slab geometry[60,61] was used with the size of the unit cell set to 30 × 30 Å × 100 Å and periodic boundary conditions in three dimensions.[62] The elongated *z*-axis is normal to two liquid–vapor interfaces. Simulations were carried out at constant volume and a constant temperature of 300 K (NVT ensemble) after equilibration in the same ensemble using the Berendsen thermostat.[63] All of the simulations were completed using the Amber 8 suite of programs.[64] Long-range electrostatic interactions were calculated using the particle mesh Ewald method[65,66] with a real space cutoff of 12 Å. Water molecules were modeled using the polarizable POL3 water model[67,68] and the internal degrees of freedom of the water molecules were constrained using the SHAKE algorithm.[68] Nitrate ions were modeled using the parameters recommended by Salvador *et al.*[69] and used in two subsequent studies on nitrate in interfacial environments.[42,43] The sodium and chloride parameters were taken from Perera and Berkowitz.[70] Simulations of pure $NaNO_3$ and mixed 1 : 1 NaCl : $NaNO_3$ were carried out for 4 ns. For mixed 9 : 1 and 1 : 9 NaCl : $NaNO_3$ slabs, the simulations were run for an additional nanosecond (5 ns total). In all cases, a timestep of 1 fs was used. In order to avoid the polarization catastrophe[71] due to the large electric field in solutions with a large number of polarizable molecules, the induced dipoles were calculated using a method developed by Jungwirth and coworkers.[72] As in prior studies, the induced dipole scaling was chosen to preserve the properties of neat POL3 water.

UV/Visible spectroscopy measurements

The UV absorption spectra of aqueous $NaNO_3$ and NaCl–$NaNO_3$ solutions were obtained using a Cary 50 UV-visible spectrophotometer at 0.5 nm resolution. UV grade quartz cells of path length 0.1 mm, 1 mm and 1 cm were used to cover the 0.4–6.0 M range of nitrate concentration. UV spectra were collected for pure $NaNO_3$ as well as mixtures with molar ratios of 1 : 9, 1 : 1, 3 : 1, and 9 : 1 NaCl : $NaNO_3$. In addition, UV spectra were taken in which the nitrate ion concentration was held constant at 0.4 M while that of Cl^- was varied from 0–3.6 M.

Kinetics analysis

A kinetics modeling program[73] was used to investigate the gas phase chemistry and its impact on the measured NO_2 concentrations. Although the photochemistry of interest occurs in the thin surface film, the observable parameters are gas phase concentrations that result from the thin film photolysis. Thus, a detailed gas phase model was developed in which the production of gas phase NO_2 from the surface nitrate ion photolysis (1a) was parameterized by matching the model to experimental NO_2 data from pure $NaNO_3$ photolysis experiments (ESI).† The channel producing nitrite ion and O atoms (reaction 1b) was then assigned a rate constant based on the known quantum yields for the two channels, *i.e.*, reaction (1b) is a factor of ~10 slower.[16,21]

Chemicals

The salts NaCl (Fluka, >99.5%), $NaNO_3$ (Fisher, Certified ACS, >99.0%), and Na_2SO_4 (Fisher, 99.9%) were used as received from the manufacturers, and solutions were made using Nanopure or Milli-Q water (≥ 18.0 MΩ cm). The backing pressure on the nebulizer was provided by N_2 gas (Oxygen Service Co., UHP, 99.999%), and aerosol photolysis experiments were carried out in Ultrapure air (Scott-Marrin, NO_x < 0.001 ppm, SO_2 < 0.001 ppm). Nitrogen dioxide was used as received (Scott-Marrin certified gas mixture, 4.57 ppm NO_2 in N_2, or 329 ppm NO_2 in He) for calibrations and test experiments. Nitric oxide (NO, Matheson, 99%) was purified before use by passing through a cold trap at ≤ −60 °C to remove NO_2 and HNO_3 impurities.

3. Results and discussion

NO_2 Production in photolysis experiments

The production of NO_2 as a function of photolysis time is shown in Fig. 2a for $NaNO_3$ and for NaCl–$NaNO_3$ mixtures with varying molar ratios. The error bars represent two sample standard deviations (2σ) of repeated experiments. As the initial concentration of $NaNO_3$ in the nebulized mixtures increases, the concentration of gas phase NO_2 produced increases, as expected.

To compare the production of NO_2 relative to the initial NO_3^- present, the data in Fig. 2a were divided by the initial NO_3^- molarity in the nebulizing solution. As shown in Fig. 2b, this normalized NO_2 increases as the relative amount of chloride increases. $NaNO_3$ in the absence of chloride produced the least amount of NO_2 per mole of initial NO_3^-, while there was a substantial enhancement in the yield of NO_2 for the irradiated 9 : 1 NaCl : $NaNO_3$ mixture. A similar trend was measured for NO production, which however, is generated at much smaller concentrations since it is not a primary photoproduct of NO_3^- photolysis.[16]

One potential explanation for this surprising result is that when chloride is present, nitrate ions are closer to the interface where a reduced solvent cage can lead to enhanced escape of nitrate ion photofragments such as NO_2 into the gas phase.

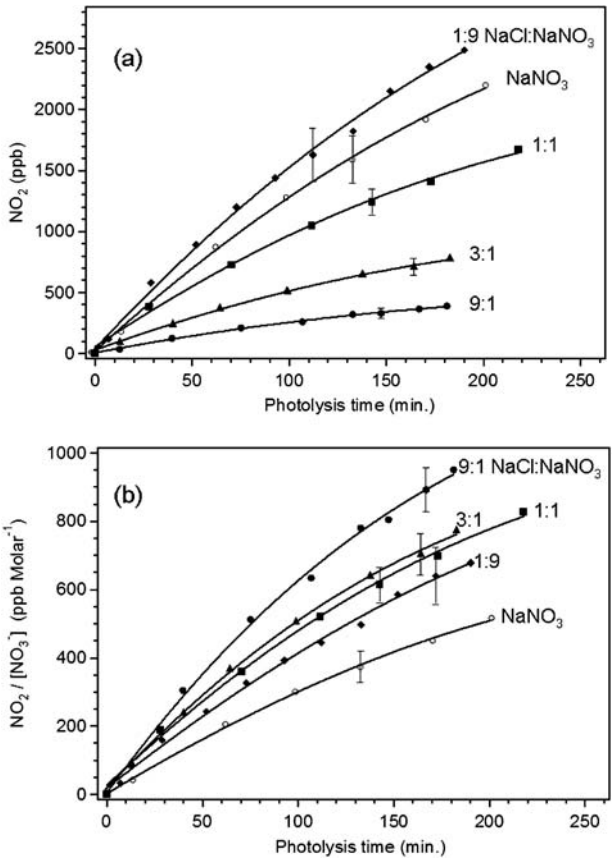

Fig. 2 (a) Measured NO_2 production from typical aerosol photolysis experiments of pure $NaNO_3$ and NaCl–$NaNO_3$ mixtures. (b) NO_2 production normalized by dividing by $[NO_3^-]_0$ in the nebulizing solution. Error bars represent typical 2σ errors of replicate experiments. Curves are least squares fits to the data.

For example, theoretical calculations by Benjamin and co-workers[48,50] suggest that photolysis of ICN at the interface leads to enhanced desorption of the photoproducts into the gas phase relative to photolysis of bulk ICN solutions due to reduced trapping by an incomplete solvent cage at the surface, and there is experimental evidence for surface-enhanced photolysis as well.[46,47,51]

Molecular dynamics simulations

To assess whether chloride ions can draw nitrate ions closer to the aqueous interface, molecular dynamics simulations were carried out on solutions of $NaNO_3$, NaCl and mixtures of the two. The goal of the simulations was to investigate ion partitioning at the liquid–vapor interface of aqueous sodium nitrate and sodium chloride mixtures, which could alter the effective quantum yield for nitrate ion photolysis. Simulations of pure aqueous sodium nitrate at two concentrations are discussed here; the reader is referred to recent work[43] on aqueous sodium nitrate in interfacial environments for more detailed structural information. In the present work, simulations of saturated $NaNO_3$, which corresponds well to the experimental conditions, are presented. Simulations on less concentrated (approximately 3.2 M $NaNO_3$) were also carried out. The number of ions in each simulation (all with 864 water molecules) is shown in Table 1.

In order to mimic mixtures that correspond to the experimental conditions, simulations of mixed $NaNO_3$ and NaCl were performed on approximately 3.2 M $NaNO_3$ with the same number of corresponding NaCl ions (*i.e.* 36 NO_3^-, 36 Cl^-, and 72 Na^+ ions; referred to as the 1 : 1 ion ratio, Table 1). Then, the total number of Na^+ ions was fixed at 72 and the anion ratios were varied to represent 1 : 9 and 9 : 1 mixtures of chloride to nitrate. The total number of ions (cations + anions) in each mixed salt simulation was 144.

Snapshots of the liquid vapor interface of 1 : 1 and 9 : 1 NaCl : $NaNO_3$ mixtures are shown in Fig. 3. Density profiles for four simulations are shown in Fig. 4. For ease of comparison, each density profile was normalized using $\int_{z_{min}}^{z_{max}} \rho(z)\mathrm{d}z = 1$, averaged about the center of the slab, and then shifted along the z-axis so that the water Gibbs dividing surface (GDS) is located at $z = 0$. For the purposes of this study, we approximate the water GDS as the z coordinate where the interfacial water density is half the bulk density. Fig. 4a for concentrated aqueous $NaNO_3$ shows that only a small amount of nitrate resides close to the liquid–vapor interface, in contrast to the significant number of chloride ions that are found at the interface (Fig. 4b).[29–32] For the system with an equal number of nitrate and chloride anions (Fig. 4c), the chloride density profile looks similar to the pure NaCl simulation,[29] while nitrate is pulled closer to the interface. In the case where the chloride to nitrate ratio is 9 : 1 (Fig. 4d), the nitrate ions are drawn markedly closer to the interface than in pure sodium nitrate. This can also be observed in the snapshots in Fig. 3 where for mixed 9 : 1 NaCl : $NaNO_3$ (Fig. 3b), nitrate ions are located near sodium ions that have been drawn toward the surface chloride ions. The density profiles for pure ~3.2 M $NaNO_3$ are not shown because they are very similar to those of the concentrated solution (Fig. 4a). For mixed 1 : 9 NaCl : $NaNO_3$ the density profiles are similar to the 1 : 1 mixture (Fig. 4c) and are also not shown.

The water solvation environment of the nitrate ions in the 9 : 1 NaCl : $NaNO_3$ was investigated by calculating the $N_{nitrate}$–O_{water} radial distribution functions at different positions of the nitrate ion relative to the Gibbs dividing surface. The radial distribution function (RDF), $g(r)$, describes the density variations of the surrounding water molecules as a function of distance from the nitrate nitrogen. The RDF in this case is used to define the relative extent of solvation of bulk *versus* near surface nitrate ions (Fig. 5). Ions located 6 Å below the GDS have a water solvation environment similar to bulk ions. However, the RDFs for nitrate ions located 3 Å and 1 Å below the GDS exhibit deviations from the bulk RDF, indicating a progressive change in the solvation environment of nitrate ions as they approach the interface. For bulk nitrate ions, there are 19.6 water molecules within 5.5 Å of $N_{nitrate}$, while nitrate ions 1 Å below the GDS are surrounded by 15.3 water molecules within the same distance. Clearly, nitrate ions located 1 Å below the water GDS do not have a complete solvation shell.

Table 1 Compositions of systems studied using MD simulations with 864 water molecules

System description	No. of chloride ions	No. of nitrate ions	No. of sodium ions
$NaNO_3$ (~6.8 M)	—	86	86
$NaNO_3$ (~3.2 M)	—	36	36
Mixed 1 : 1 NaCl : $NaNO_3$	36	36	72
Mixed 1 : 9 NaCl : $NaNO_3$	7	65	72
Mixed 9 : 1 NaCl : $NaNO_3$	65	7	72

Previous experimental and theoretical studies have shown that photolysis of aerosols in which the solute has a reduced solvent cage can increase the yield of products.[46–51] Enhanced production of gas phase NO_2 could therefore be expected in the presence of chloride ions which draw NO_3^- closer to the interface *via* the electric double layer with Na^+. This is consistent with the data in Fig. 2b that show enhanced production of gas phase NO_2 in chloride–nitrate mixtures. The measured NO_2 yields from the 1 : 1 and 1 : 9 NaCl : $NaNO_3$ solutions are within experimental error of each other, and this is also consistent with MD simulations, which predicted similar distributions of NO_3^- in these mixtures.

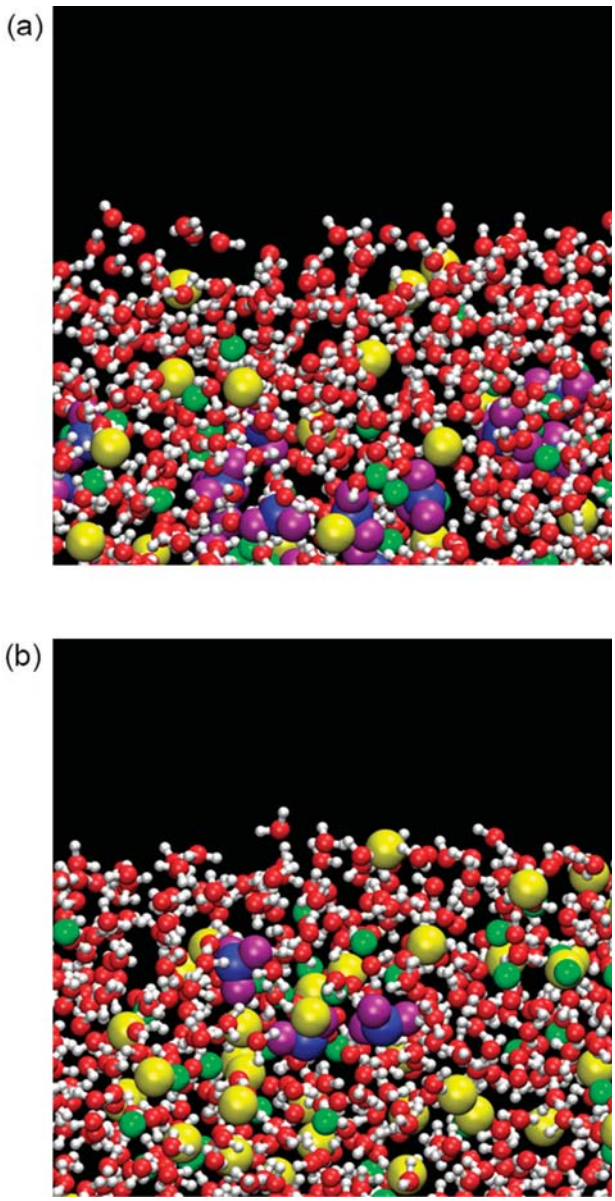

Fig. 3 Snapshots of side views of configurations from MD simulations of mixed aqueous $NaNO_3$ and NaCl. In panel (a) the ratio is 1 : 1 NaCl : $NaNO_3$ and in (b) the ratio is 9 : 1 NaCl : $NaNO_3$. Only half of the slab is shown for each system, and the snapshots are oriented such that the bulk solution is at the bottom of each panel. Colour legend: green = Na^+, yellow = Cl^-, blue = N, purple = $O_{nitrate}$, red = O_{water}, white = H_{water}.

UV/Visible spectroscopy measurements

Another potential source of the enhanced photochemistry in the presence of chloride ions is a shift in the nitrate UV absorption spectrum in the salt mixtures. For example, a red-shift of the $n \rightarrow \pi^*$ transition in NO_3^- with increasing Cl^- concentrations would give increased overlap of the nitrate absorption and the photolysis lamp (Fig. 1), leading to increased photolysis. An increase in the NO_3^- absorption coefficient with increasing Cl^- concentrations would lead to the same effect. To investigate these possibilities, UV absorption spectra were measured for $NaNO_3$ solutions and for mixed NaCl–$NaNO_3$ solutions used to generate aerosols in the photolysis experiments.

Fig. 6 shows the molar absorption coefficients measured for a 4 M $NaNO_3$ solution and for a mixture of 0.4 M $NaNO_3$ and 3.6 M NaCl for which enhanced photochemical production of NO_2 was observed (Fig. 2). There is no significant difference between these absorption spectra, ruling out a shift or increase in the nitrate absorption due to the presence of chloride as the source of the enhanced photochemistry. A spectrum of dilute, aqueous $NaNO_3$ is also included in Fig. 6 (0.4 M, dashed line) for reference. Increased concentrations of $NaNO_3$ cause small blue-shifts of ~1–2 nm relative to dilute $NaNO_3$. This shift is slightly smaller than the 2–4 nm shift for $NaNO_3$ up to ~7 M reported by Hudson *et al.*[28] Interestingly, the addition of high concentrations of NaCl (3.6 M) to dilute (0.4 M) $NaNO_3$ causes a similar shift, suggesting it is due to an ionic strength effect.

NO_2 Enhancement and kinetics analysis

As a further test that the observed enhancement is due to Cl^-, another salt was chosen to mix with $NaNO_3$. If nitrate ions are drawn closer to the interface due to the significant interfacial concentration of the Cl^- anion, then solutions of nitrate with an anion that prefers bulk solvation should not exhibit enhanced NO_2 yields. A photolysis experiment was carried out using aerosols nebulized from a 1 : 1 Na_2SO_4 : $NaNO_3$ solution.

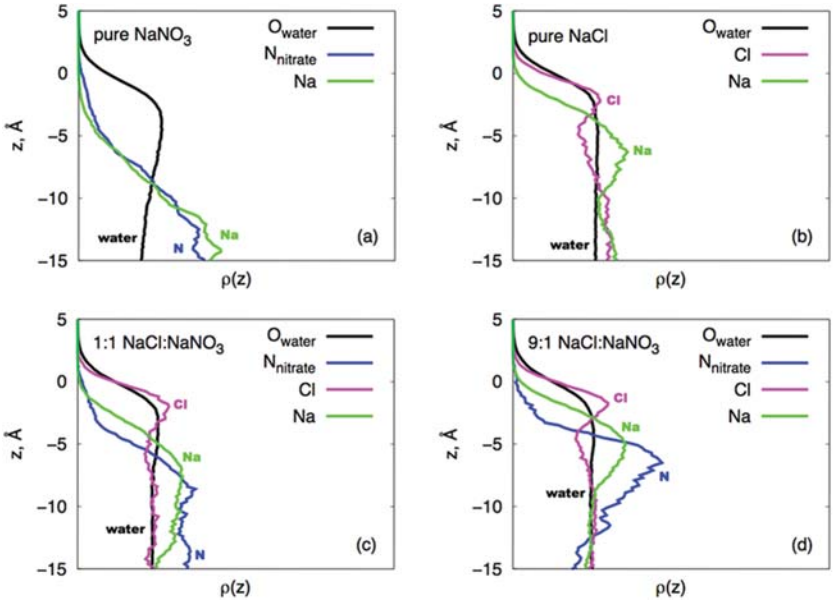

Fig. 4 Density profiles for simulations of the air–water interface of (a) ~6.8 M aqueous $NaNO_3$, (b) ~3 M NaCl, and (c) and (d) mixed solutions of $NaNO_3$ and NaCl.

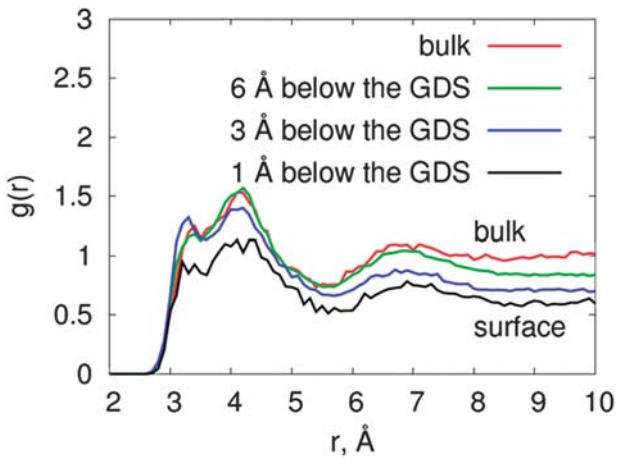

Fig. 5 $N_{nitrate}$–O_{water} radial distribution functions for the 9 : 1 NaCl : $NaNO_3$ mixture shown for several distances of the nitrate from the Gibbs dividing surface. Note that near the surface of the solution (~1 Å below the GDS), the nitrate ions are undercoordinated relative to the bulk.

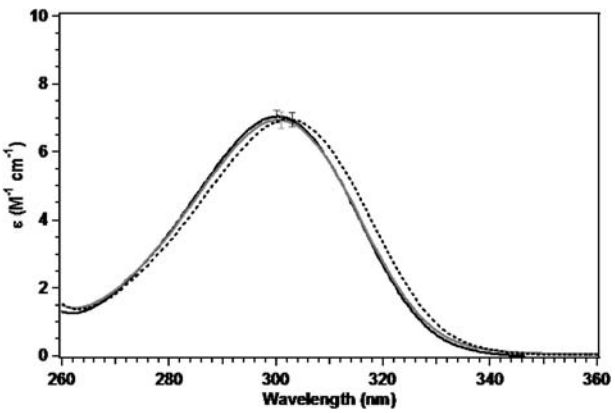

Fig. 6 UV/visible spectra of 4.0 M $NaNO_3$ (solid black line), 3.6 M NaCl : 0.4 M $NaNO_3$ mixture (gray), and 0.4 M $NaNO_3$ (dashed). Error bars represent 2σ of repeat measurements (3–4%).

Molecular dynamics simulations of Na_2SO_4 solutions show that SO_4^{2-} prefers bulk solvation over the interface.[74] In addition, Na_2SO_4 does not photolyze in the wavelength region used in the current studies, thus it is expected to act only as a spectator ion. Due to the lower solubility of Na_2SO_4, the solution was 0.8 M Na_2SO_4 : 0.8 M $NaNO_3$. The NO_2 measurements as a function of photolysis time were divided by this initial NO_3^- concentration for comparison to NaCl–$NaNO_3$ experiments. This normalized rate of experimental NO_2 formation was in excellent agreement with those of pure $NaNO_3$, *i.e.*, no enhancement was observed, confirming that Cl^- is important in inducing the enhancement.

For each NaCl : $NaNO_3$ ratio, the normalized rates of NO_2 formation were used to calculate the amount of NO_2 enhancement relative to pure $NaNO_3$. The initial rate of NO_2 formation was determined by taking the initial slope of each normalized NO_2-time series in Fig. 2b. The enhancement is expressed as the ratio of the initial rate for each NaCl : $NaNO_3$ mixture to that for pure $NaNO_3$, such that pure $NaNO_3$ has an "enhancement" of 1.0. The NO_2 enhancements, shown in Fig. 7, ranged from ~1.6–1.8 for lower NaCl : $NaNO_3$ ratios (1 : 9, 1 : 1, 3 : 1) to 2.4 for the highest NaCl : $NaNO_3$ ratio of 9 : 1. The enhancement for the Na_2SO_4–$NaNO_3$ experiment, 0.97, is also included in the plot and is within experimental error of pure $NaNO_3$. Table 2 summarizes the initial rates of NO_2 formation and the calculated enhancements in the production of gas phase NO_2.

The use of initial rates minimizes secondary chemistry that may occur, forming additional oxides of nitrogen that can

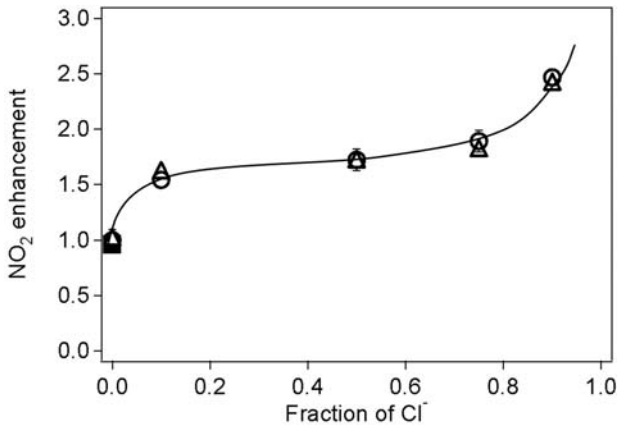

Fig. 7 Plot of the NO_2 enhancement factors obtained from initial rates of NO_2 formation (open circles, $\pm 2\sigma$ errors) as a function of the fraction of Cl^- in the solution. Triangles are the model-predicted enhancement factors. The closed square is the enhancement observed for the mixed $NaSO_4$–$NaNO_3$ experiment. The curve is a guide for the eye only.

interfere in the NO_y analyzer.[75–77] Kinetics modeling, which includes the known secondary chemistry of oxides of nitrogen (ESI Table S-1), was also used to determine the NO_2 enhancement for each $NaCl:NaNO_3$ ratio. The solid lines in Fig. 8 show the model-predicted NO_y for several typical experiments. The enhancements predicted by the model for each $NaCl:NaNO_3$ ratio are very similar to those calculated using initial rates of NO_2 (Fig. 7 and Table 2).

The model was also used to predict other NO_y compounds that might be measured as NO_2, *i.e.*, that would be reduced to NO over the converter in the chemiluminescence instrument. $ClNO_2$ was predicted to be the dominant interfering species, accounting for between 18% of the total NO_y predicted (for the 1 : 9 $NaCl:NaNO_3$ case) to 29% (for the 9 : 1 $NaCl:NaNO_3$ case). Concentrations of gaseous HNO_3, HONO, ClNO and $ClONO_2$ combined were predicted to build up to $<5\%$ of the total $[NO_y]$.

The OH radical should also be generated in reaction (1a), along with NO_2. However, the modeling studies showed that the overwhelming source of OH in this system was due to the formation and photolysis of O_3 to generate $O(^1D)$ which reacts with water vapor to form OH. Direct OH production from the nitrate ion photochemistry paralleling that of the NO_2 is predicted to be too small to detect.

In summary, studies of irradiation of $NaCl:NaNO_3$ aerosol mixtures showed an enhanced yield of NO_2 as the $NaCl:NaNO_3$ ratio increased. MD simulations showed that high relative concentrations of Cl^- attract the Na^+ cations to the subsurface which, in turn, attract NO_3^- to the subsurface. The combined experimental and theoretical results show that a reduced solvent cage for subsurface NO_3^- is responsible for the enhanced NO_2 yields. This enhancement of NO_2 does not occur for mixtures of Na_2SO_4–$NaNO_3$ due to the preferred bulk solvation of the SO_4^{2-} ion, which does not lead to an interfacial double layer.

Atmospheric implications

The studies presented here show that the presence of chloride ions can alter the photochemical yield of gaseous NO_2 from NO_3^- photolysis due to reduced solvent cage effects. The present studies may actually underestimate this effect in airborne sea salt particles, where the particle sizes can be smaller and hence surface effects more pronounced. Even in the absence of Cl^- or other ions that may draw NO_3^- toward the interface, the MD simulations show that quantum yields measured using bulk solutions may underpredict NO_x generation from NO_3^- photolysis due to the under-coordination of NO_3^- at interfaces. Photochemical enhancement of NO_3^- photolysis may also occur with other anions, including organics,[78] that are often present in particles or on snowpacks.[25,79–83]

The photolysis of nitrate has been proposed to be a major source of NO_x in snowpacks, where surprisingly high levels of oxides of nitrogen and photochemical activity have been measured.[22–25,55,84–88] Model studies of this process assume that the absorption cross sections and quantum yields measured for pure $NaNO_3$ can be applied to the atmosphere, including the air within the snowpack. However, snowpacks and frost flowers also contain halide ions from sea spray deposited on the ice,[89–93] whose surface is believed to be a quasi-liquid layer.[94–96] Given the large chloride ion content of sea spray, the quantum yields for nitrate photolysis may be significantly larger than assumed based on nitrate alone. This would increase the rate of production of NO_2 within the snowpack.

In addition, as discussed above, predictions of NO_x from NO_3^- photolysis, based on quantum yields measured from *bulk* NO_3^- solutions, will increase due to the presence of

Table 2 Measured initial rates of formation of NO_2 divided by initial $[NO_3^-]$ and enhancement factors from initial formation rates and kinetics modeling

System description	Average initial rates of NO_2 formation divided by $[NO_3^-]_0$ ($\pm 2\sigma$)[b]/ppb min^{-1} M^{-1}	NO_2 Enhancement factor ($\pm 2\sigma$)[a] from initial rates[b]	NO_2 Enhancement factor from kinetics modeling
$NaNO_3$	3.0 ± 0.4	1.0 ± 0.1	1.0
1 : 9 $NaCl:NaNO_3$	4.8 ± 0.04	1.6 ± 0.01	1.6
1 : 1 $NaCl:NaNO_3$	5.3 ± 0.2	1.8 ± 0.1	1.7
3 : 1 $NaCl:NaNO_3$	5.8 ± 0.2	1.9 ± 0.1	1.8
9 : 1 $NaCl:NaNO_3$	7.6 ± 0.07	2.5 ± 0.02	2.4
1 : 1 $Na_2SO_4:NaNO_3$	2.9 ± 0.15	0.97 ± 0.05	1.0

[a] 2σ represents two sample standard deviations. [b] Enhancement relative to $NaNO_3$ only, obtained by dividing by average initial rate of NO_2 formation from $NaNO_3$ only system.

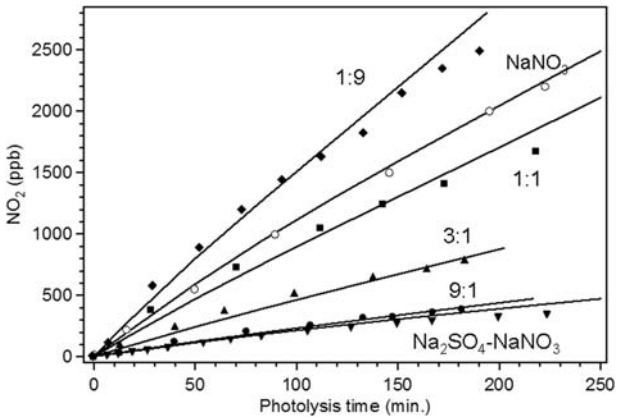

Fig. 8 Kinetics modeling fits (lines) to experimental data (symbols) for typical photolysis experiments.

under-coordinated NO_3^- at interfaces where incomplete solvent shells lead to enhanced photochemistry. Furthermore, under acidic conditions the nitrite generated in reaction (1b) will be protonated to form HONO, so that the rate of HONO production may also be larger than expected due to the presence of chloride.

In the case of particles in polluted air, while the additional NO_2 produced by the enhancement is expected to be minor relative to ambient concentrations, the accompanying OH produced near the interface may oxidize organics present in or on the particle.[97] Similar oxidations by OH generated at the interface may occur in the snowpack as well.

While the present studies were directed to chloride–nitrate mixtures, sea spray also contains bromide which plays an important role in the Arctic at polar sunrise[98–103] and likely at lower latitudes as well.[104,105] Bromide ion enhancement at the interface has been shown theoretically and experimentally to be greater than that for chloride ions.[29–31,34,37,106] It is therefore expected that bromide ions will be even more effective in pulling nitrate ions towards the interface through the double-layer effect and that the quantum yields will be greater than for the chloride–nitrate mixtures.

Finally, although we could not directly observe enhanced OH production in this system, it should be occurring simultaneously with the increased NO_2 generation. Given the presence of organic coatings on sea salt particles,[79–83] oxidation of such coatings "from the bottom up" may occur for aged sea salt particles containing mixtures of chloride, bromide and nitrate. Studies are underway to probe this possibility as well as the enhanced photochemistry in bromide–nitrate mixtures.

Acknowledgements

This research was supported by the National Science Foundation (Grant # ATM-0423804), the US Department of Energy (Grant # DE-FG02-05ER64000) and AirUCI, an Environmental Molecular Sciences Institute funded by the National Science Foundation (Grant # CHE-0431512). MR gratefully acknowledges support from the Ministry of Education of the Czech Republic (Grants 1P05ME798 and LC512). The work in Prague was performed within the framework of the research project Z40550506. The authors are grateful to Mike Ezell, Yong Yu, and James N. Pitts, Jr. for insightful discussions.

References

1 W. H. Schroeder and P. Urone, *Environ. Sci. Technol.*, 1974, **8**, 756.
2 B. J. Finlayson-Pitts, *Nature*, 1983, **306**, 676.
3 B. J. Finlayson-Pitts, M. J. Ezell and J. N. Pitts, Jr, *Nature*, 1989, **337**, 241.
4 D. C. S. Beddows, R. J. Donovan, R. M. Harrison, M. R. Heal, R. P. Kinnersley, M. D. King, D. H. Nicholson and K. C. Thompson, *J. Environ. Monit.*, 2004, **6**, 124.
5 M. Dall'Osto, D. C. S. Beddows, R. P. Kinnersley and R. M. Harrison, *J. Geophys. Res., [Atmos.]*, 2004, **109**, DOI: 10.1029/2004JD004747.
6 B. J. Finlayson-Pitts and J. N. Pitts, Jr, *Chemistry of the Upper and Lower Atmosphere—Theory, Experiments, and Applications*, Academic Press, San Diego, 2000.
7 E. E. Gard, M. J. Kleeman, D. S. Gross, L. S. Hughes, J. O. Allen, B. D. Morrical, D. P. Fergenson, T. Dienes, M. E. Galli, R. J. Johnson, G. R. Cass and K. A. Prather, *Science*, 1998, **279**, 1184.
8 A. Laskin, M. J. Iedema and J. P. Cowin, *Environ. Sci. Technol.*, 2002, **36**, 4948.
9 T. A. Pakkanen, *Atmos. Environ.*, 1996, **30**, 2475.
10 R. von Glasow and P. J. Crutzen, Tropospheric Halogen Chemistry, in *Treatise on Geochemistry, Update 1*, ed. H. D. Holland and K. Turekian, 2007, vol. 4.02, p. 1.
11 J. R. Arnold and W. T. Luke, *Atmos. Environ.*, 2007, **41**, 4227.
12 P. K. Dasgupta, S. W. Campbell, R. S. Al-Horr, S. M. R. Ullah, J. Li, C. Amalfitano and N. D. Poor, *Atmos. Environ.*, 2007, **41**, 4242.
13 B. J. Finlayson-Pitts and J. C. Hemminger, *J. Phys. Chem. A*, 2000, **104**, 11463.
14 B. J. Finlayson-Pitts, *Chem. Rev.*, 2003, **103**, 4801.
15 M. J. Rossi, *Chem. Rev.*, 2003, **103**, 4823.
16 J. Mack and J. R. Bolton, *J. Photochem. Photobiol., A*, 1999, **128**, 1.
17 R. G. Zepp, J. Hoigne and H. Bader, *Environ. Sci. Technol.*, 1987, **21**, 443.
18 R. Zellner, M. Exner and H. Herrmann, *J. Atmos. Chem.*, 1990, **10**, 411.
19 P. Warneck and C. Wurzinger, *J. Phys. Chem.*, 1988, **92**, 6278.
20 A. Alif and P. Boule, *J. Photochem. Photobiol., A*, 1991, **59**, 357.
21 H. Herrmann, *Phys. Chem. Chem. Phys.*, 2007, **9**, 3935.
22 A. L. Sumner and P. B. Shepson, *Nature*, 1999, **398**, 230.
23 R. E. Honrath, M. C. Peterson, S. Guo, J. E. Dibb, P. B. Shepson and B. Campbell, *Geophys. Res. Lett.*, 1999, **26**, 695.
24 R. E. Honrath, M. C. Peterson, M. P. Dziobak, J. E. Dibb, M. A. Arsenault and S. A. Green, *Geophys. Res. Lett.*, 2000, **27**, 2237.
25 A. M. Grannas, A. E. Jones, J. Dibb, M. Ammann, C. Anastasio, H. J. Beine, M. Bergin, J. Bottenheim, C. S. Boxe, G. Carver, G. Chen, J. H. Crawford, F. Domine', M. M. Frey, M. I. Guzman, D. E. Heard, D. Helmig, M. R. Hoffmann, R. E. Honrath, L. G. Huey, M. Hutterli, H. W. Jacobi, P. Klan, B. Lefer, J. McConnell, J. Plane, R. Sander, J. Savarino, P. B. Shepson, W. R. Simpson, J. R. Sodeau, R. von Glasow, R. Weller, E. W. Wolff and T. Zhu, *Atmos. Chem. Phys.*, 2007, **7**, 4329.
26 R. C. Hoffman, A. Laskin and B. J. Finlayson-Pitts, *J. Aero Sci.*, 2004, **35**, 869.
27 M. E. Wise, T. A. Semeniuk, R. Bruintjes, S. T. Martin, L. M. Russel and P. R. Buseck, *J. Geophys. Res., [Atmos.]*, 2007, **112**, D10224.
28 P. K. Hudson, J. Schwarz, J. Baltrusaitis, E. R. Gibson and V. H. Grassian, *J. Phys. Chem. A*, 2007, **111**, 544.
29 P. Jungwirth and D. J. Tobias, *J. Phys. Chem. B*, 2001, **105**, 10468.
30 P. Jungwirth and D. J. Tobias, *J. Phys. Chem. B*, 2002, **106**, 6361.
31 P. Jungwirth and D. J. Tobias, *Chem. Rev.*, 2006, **106**, 1259.
32 E. M. Knipping, M. J. Lakin, K. L. Foster, P. Jungwirth, D. J. Tobias, R. B. Gerber, D. Dabdub and B. J. Finlayson-Pitts, *Science*, 2000, **288**, 301.
33 E. M. Knipping and D. Dabdub, *J. Geophys. Res., [Atmos.]*, 2002, **107**, DOI: 10.1029/2001JD000867.

34 S. W. Hunt, M. Roeselová, W. Wang, L. M. Wingen, E. M. Knipping, D. J. Tobias, D. Dabdub and B. J. Finlayson-Pitts, *J. Phys. Chem. A*, 2004, **108**, 11559.
35 S. Pechtl and R. von Glasow, *Geophys. Res. Lett.*, 2007, **34**, L11813, DOI: 10.1029/2007GL029761.
36 W. C. Keene, J. Stutz, A. A. P. Pszenny, J. R. Maben, E. V. Fischer, A. M. Smith, R. von Glasow, S. Pechtl, B. C. Sive and R. K. Varner, *J. Geophys. Res., [Atmos.]*, 2007, **112**, DOI: 10.1029/2006JD007689.
37 S. Ghosal, J. C. Hemminger, H. Bluhm, B. S. Mun, E. Hebenstreit, G. Ketteler, F. Ogletree, F. Requejo and M. Salmeron, *Science*, 2005, **307**, 563.
38 J. Cheng, C. D. Vecitis, M. R. Hoffmann and A. J. Colussi, *J. Phys. Chem. B*, 2006, **110**, 25598.
39 M. Krisch, R. D'Auria, M. A. Brown, D. J. Tobias, J. C. Hemminger, M. Ammann, D. E. Starr and H. Bluhm, *J. Phys. Chem. C*, 2007, **111**, 13497.
40 J.-H. Kim, Y.-K. Kim and H. Kang, *J. Phys. Chem. C*, 2007, **111**, 8030.
41 P. B. Petersen and R. J. Saykally, *Chem. Phys. Lett.*, 2004, **397**, 51.
42 B. Minofar, R. Vacha, A. Wahab, S. Mahiuddin, W. Kunz and P. Jungwirth, *J. Phys. Chem. B*, 2006, **110**, 15939.
43 J. L. Thomas, M. Roeselová, L. X. Dang and D. J. Tobias, *J. Phys. Chem. A*, 2007, **111**, 3091.
44 D. E. Otten, P. B. Petersen and R. J. Saykally, *Chem. Phys. Lett.*, 2007, **449**, 261.
45 Y. Miller, J. L. Thomas, D. D. Kemp, B. J. Finlayson-Pitts, M. S. Gordon, D. J. Tobias and R. B. Gerber, 2008, in preparation.
46 J. D. Graham, J. T. Roberts, L. D. Anderson and V. H. Grassian, *J. Phys. Chem.*, 1996, **100**, 19551.
47 A. Furlan, *J. Phys. Chem. B*, 1999, **103**, 1550.
48 J. Vieceli, I. Chorny and I. Benjamin, *J. Chem. Phys.*, 2001, **115**, 4819.
49 I. Chorny, J. Vieceli and I. Benjamin, *J. Phys. Chem. B*, 2003, **107**, 229.
50 N. Winter and I. Benjamin, *J. Chem. Phys.*, 2004, **121**, 2253.
51 P. Nissenson, C. J. H. Knox, B. J. Finlayson-Pitts, L. F. Phillips and D. Dabdub, *Phys. Chem. Chem. Phys.*, 2006, **8**, 4700.
52 A. Laskin, H. Wang, W. H. Robertson, J. P. Cowin, M. J. Ezell and B. J. Finlayson-Pitts, *J. Phys. Chem. A*, 2006, **110**, 10619.
53 X.-Y. Yu and J. R. Barker, *J. Phys. Chem. A*, 2003, **107**, 1313.
54 G. L. Petriconi, E. G. Gori, A. C. Montefinale and H. M. Papee, Photolytic Release of Hygroscopic Material from Nitrate-Bearing Aerosol, , in *Proceedings of the International Conference on Cloud Physics*, 1968, vol. 1.3, p. 15.
55 C. Anastasio and J. T. Newberg, *J. Geophys. Res., [Atmos.]*, 2007, **112**, D10306.
56 T. Arakaki, Y. Kuroki, K. Okada, Y. Nakama, H. Ikota, M. Kinjo, T. Higuchi, M. Uehara and A. Tanahara, *Atmos. Environ.*, 2006, **40**, 4764.
57 I. N. Tang and H. R. Munkelwitz, *J. Geophys. Res., [Atmos.]*, 1994, **99**, 18801.
58 Z. Ge, A. S. Wexler and M. V. Johnston, *J. Phys. Chem. A*, 1998, **102**, 173.
59 A. S. Wexler and J. H. Seinfeld, *Atmos. Environ.*, 1991, **25A**, 2731.
60 M. A. Wilson, A. Pohorille and L. R. Pratt, *J. Phys. Chem.*, 1987, **91**, 4873.
61 I. Benjamin, *J. Chem. Phys.*, 1991, **95**, 3698.
62 M. P. Allen and D. J. Tildesley, *Computer Simulation of Liquids*, Clarendon, Oxford, 1987.
63 H. J. C. Berendsen, J. P. M. Postma, W. F. Vangunsteren, A. Dinola and J. R. Haak, *J. Chem. Phys.*, 1984, **81**, 3684.
64 D. A. Case, T. A. Darden, T. E. Cheatham, III, C. L. Simmerling, J. Wang, R. E. Duke, R. Luo, K. M. Merz, B. Wang, D. A. Pearlman, M. Crowley, S. Brozell, V. Tsui, H. Gohlke, J. Mongan, V. Hornak, G. Cui, P. Beroza, C. Schafmeister, J. W. Caldwell, W. S. Ross and P. A. Kollman, *AMBER 8*, University of California, San Francisco, 2004.
65 T. Darden, D. York and L. Pedersen, *J. Chem. Phys.*, 1993, **98**, 10089.
66 U. Essmann, L. Perera, M. L. Berkowitz, T. Darden, H. Lee and L. G. Pedersen, *J. Chem. Phys.*, 1995, **103**, 8577.
67 J. W. Caldwell and P. A. Kollman, *J. Phys. Chem.*, 1995, **99**, 6208.
68 J. P. Ryckaert, G. Ciccotti and H. J. C. Berendsen, *J. Comput. Phys.*, 1977, **23**, 327.
69 P. Salvador, J. E. Curtis, D. J. Tobias and P. Jungwirth, *Phys. Chem. Chem. Phys.*, 2003, **5**, 3752.
70 L. Perera and M. L. Berkowitz, *J. Chem. Phys.*, 1994, **100**, 3085.
71 B. T. Thole, *Chem. Phys.*, 1981, **59**, 341.
72 P. B. Petersen, R. J. Saykally, M. Mucha and P. Jungwirth, *J. Phys. Chem. B*, 2005, **109**, 10915.
73 W. Braun, J. T. Herron and D. K. Kahaner, *Int. J. Chem. Kinet.*, 1988, **20**, 51.
74 S. Gopalakrishnan, P. Jungwirth, D. J. Tobias and H. C. Allen, *J. Phys. Chem. B*, 2005, **109**, 8861.
75 J. Bradshaw, S. Sandholm and R. Talbot, *J. Geophys. Res., [Atmos.]*, 1998, **103**, 19129.
76 D. A. V. Kliner, B. C. Daube, J. D. Burley and S. C. Wofsy, *J. Geophys. Res., [Atmos.]*, 1997, **102**, 10759.
77 E. Sanhueza, C. N. Plum and J. N. Pitts, Jr, *Atmos. Environ.*, 1984, **18**, 1029.
78 C. Minero, V. Maurino, F. Bono, E. Pelizzetti, A. Marinoni, G. Mailhot, M. E. Carlotti and D. Vione, *Chemosphere*, 2007, **68**, 2111.
79 H. Tervahattu, K. Hartonen, V.-M. Kerminen, K. Kupiainen, P. Aarnio, T. Koskentalo, A. F. Tuck and V. Vaida, *J. Geophys. Res., [Atmos.]*, 2002, **107**, 4053.
80 H. Tervahattu, J. Juhanoja and K. Kupiainen, *J. Geophys. Res., [Atmos.]*, 2002, **107**, 4319.
81 H. Tervahattu, J. Juhanoja, V. Vaida, A. F. Tuck, J. V. Niemi, K. Kupiainen, M. Kulmala and H. Vehkamaki, *J. Geophys. Res., [Atmos.]*, 2005, **110**, DOI: 10.1029/2004JD005400.
82 G. B. Ellison, A. F. Tuck and V. Vaida, *J. Geophys. Res., [Atmos.]*, 1999, **104**, 11633.
83 Y. Rudich, *Chem. Rev.*, 2003, **103**, 5097.
84 R. E. Honrath, S. Guo, M. C. Peterson, M. P. Dziobak, J. E. Dibb and M. A. Arsenault, *J. Geophys. Res., [Atmos.]*, 2000, **105**, 24183.
85 X. Zhou, H. J. Beine, R. E. Honrath, J. D. Fuentes, W. Simpson, P. B. Shepson and J. W. Bottenheim, *Geophys. Res. Lett.*, 2001, **28**, 4087.
86 D. Davis, J. B. Nowak, G. Chen, M. Buhr, R. Arimoto, A. Hogan, F. Eisele, L. Mauldin, D. Tanner, R. Shetter, B. Lefer and P. McMurry, *Geophys. Res. Lett.*, 2001, **28**, 3625.
87 A. E. Jones, R. Weller, P. S. Anderson, H.-W. Jacobi, E. W. Wolff, O. Schrems and H. Miller, *Geophys. Res. Lett.*, 2001, **28**, 1499.
88 E. W. Wolff, A.E. Jones, T. J. Martin and T. C. Grenfell, *Geophys. Res. Lett.*, 2002.
89 D. Toom-Sauntry and L. A. Barrie, *Atmos. Environ.*, 2002, **36**, 2683.
90 A. M. Rankin, E. W. Wolff and S. Martin, *J. Geophys. Res., [Atmos.]*, 2002, **107**, DOI: 10.1029/2002JD002492.
91 W. R. Simpson, L. Alvarez-Aviles, T. A. Douglas, M. Sturm and F. Domine, *Geophys. Res. Lett.*, 2005, **32**, DOI: 10.1029/2004GL021748.
92 W. R. Simpson, R. von Glasow, K. Riedel, P. Anderson, P. Ariya, J. Bottenheim, J. Burrows, L. Carpenter, U. Frieb, M. E. Goodsite, D. Heard, M. Hutterli, H.-W. Jacoi, L. Kaleschke, B. Neff, J. Plane, U. Platt, A. Richter, H. Roscoe, R. Sander, P. Shepson, J. Sodeau, A. Steffen, T. Wagner and E. Wolff, *Atmos. Chem. Phys. Discuss.*, 2007, **7**, 4375.
93 F. Domine, R. Sparapani, A. Ianniello and H. J. Beine, *Atmos. Chem. Phys.*, 2004, **4**, 2259.
94 T. Koop, A. Kapilashrami, L. T. Molina and M. J. Molina, *J. Geophys. Res., [Atmos.]*, 2000, **105**, 26393.
95 H. Cho, P. B. Shepson, L. A. Barrie, J. P. Cowin and R. Zaveri, *J. Phys. Chem. B*, 2002, **106**, 11226.
96 A. Bogdan, M. Kulmala, A. R. MacKenzie and A. Laaksonen, *J. Geophys. Res., [Atmos.]*, 2003, **108**, DOI: 10.1029/2002JD002606.
97 Y. Yu, M. J. Ezell, A. Zelenyuk, D. Imre, L. Alexander, J. Ortega, J. L. Thomas, K. Gogna, D. J. Tobias, B. D'Anna, C. W. Harmon, S. N. Johnson and B. J. Finlayson-Pitts, *Phys. Chem. Chem. Phys.*, 2008, **10**, 3063, DOI: 10.1039/b719495a.
98 L. A. Barrie, J. W. Bottenheim, R. C. Schnell, P. J. Crutzen and R. A. Rasmussen, *Nature*, 1988, **334**, 138.

99 L. Barrie and U. Platt, *Tellus*, 1997, **49B**, 450.
100 C. W. Spicer, R. A. Plastridge, K. L. Foster, B. J. Finlayson-Pitts, J. W. Bottenheim, A. M. Grannas and P. B. Shepson, *Atmos. Environ.*, 2002, **36**, 2721.
101 K. L. Foster, R. A. Plastridge, J. W. Bottenheim, P. B. Shepson, B. J. Finlayson-Pitts and C. W. Spicer, *Science*, 2001, **291**, 471.
102 B. J. Finlayson-Pitts and S. N. Johnson, *Atmos. Environ.*, 1988, **22**, 1107.
103 B. J. Finlayson-Pitts, F. E. Livingston and H. N. Berko, *Nature*, 1990, **343**, 622.
104 I. Nagao, K. Matsumoto and H. Tanaka, *Geophys. Res. Lett.*, 1999, **26**, 3377.
105 R. R. Dickerson, K. P. Rhoads, T. P. Carsey, S. J. Oltmans, J. P. Burrows and P. J. Crutzen, *J. Geophys. Res., [Atmos.]*, 1999, **104**, 21385.
106 J.-H. Kim, Y.-K. Kim and H. Kang, *J. Phys. Chem. C*, 2007, **111**, 8030.